Journal of Power Sources 255 (2014) 318–324

Contents lists available at ScienceDirect

Journal of Power Sources

journal homepage: www.elsevier.com/locate/jpowsour

Ball-milling preparation of one-dimensional Co–carbon nanotube and Co–carbon nanofiber core/shell nanocomposites with high electrochemical hydrogen storage ability

Cheng Chang [a], Peng Gao [a,*], Di Bao [a], Longqiang Wang [a], Ying Wang [a], Yujin Chen [b,*], Xiaoming Zhou [a], Shuchao Sun [a], Guobao Li [c], Piaoping Yang [a,*]

[a] Micro&Nano Material Research Institute, College of Materials Science and Chemical Engineering, Harbin Engineering University, Harbin 150001, PR China
[b] College of Science, Harbin Engineering University, Harbin, Heilongjiang 150001, PR China
[c] Beijing National Laboratory for Molecular Sciences, Peking University, PR China

HIGHLIGHTS

- 1D CNT (CNF)/Co nanocomposites were synthesized by a ball-milling method.
- Co shell with diameter of 4 nm has been successfully coated on CNT.
- The composites exhibited good hydrogen storage performance.

GRAPHICAL ABSTRACT

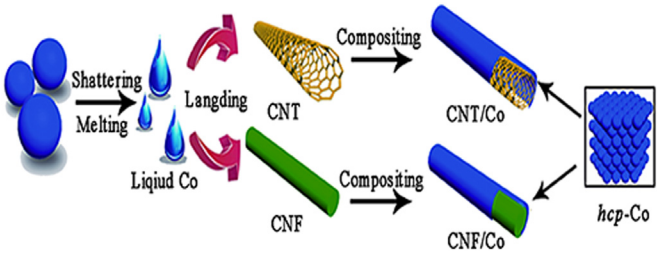

ARTICLE INFO

Article history:
Received 20 November 2013
Received in revised form
30 December 2013
Accepted 8 January 2014
Available online 15 January 2014

Keywords:
One-dimensional Co–carbon nanocomposites
Ball-milling
Core–shell structure
Layer-by-layer growth
Electrochemical hydrogen storage

ABSTRACT

Owing to the special honeycomb structures and excellent electrical characters of carbon nanotube (CNT) and carbon nanofiber (CNF), they are extensively considered as ideal cornerstones for hydrogen storage materials. Herein, metal cobalt has been uniformly coated on CNT's and CNF's surfaces in nanoscale through a simple ball milling process. Accordingly their X-ray diffraction, scanning electron microscope and transmission electron microscopy measurements clarify the satisfying composite structures. And their electrochemical experimental results demonstrate that the as-obtained CNT/Co and CNF/Co composites have excellent electrochemical hydrogen storage reversibility and considerably high storage capacities of 717.3 mAh g^{-1} (2.62 wt% hydrogen) and 739.4 mAh g^{-1} (2.70 wt% hydrogen) under room temperature and ambient pressure, which are much higher than the capacities of individual CNT (29.9 mAh g^{-1}, 0.11 wt% hydrogen) and CNF (49.0 mAh g^{-1}, 0.18 wt% hydrogen) measured in this work. Furthermore their hydrogen storage processes and the mechanism have also been investigated, in which the quasi-reversible CNT (CNF)/Co ↔ CNT (CNF)/Co–H_x reaction is the dominant cycle process.

1. Introduction

Recently the research on energy materials is of utmost importance regarding for energy harvest and energy storage. Hydrogen, as a renewable resource free of pollution, is very promising for application in future. However, the major impediment is that it is difficult to be high-capacity stored within an effective, safe and

* Corresponding authors. Tel.: +86 13224615818.
E-mail addresses: gaopeng@hrbeu.edu.cn (P. Gao), chenyujin@hrbeu.edu.cn (Y. Chen), yangpiaoping@hrbeu.edu.cn (P. Yang).

0378-7753/$ – see front matter © 2014 Elsevier B.V. All rights reserved.
http://dx.doi.org/10.1016/j.jpowsour.2014.01.034

stable solid-state medium, which restricts its practical application [1–4]. So highly efficient and convenient hydrogen storage materials and technologies become challenges for today's development of hydrogen economy [5–7]. Therefore, many storage mediums have been developed to uptake as much as possible hydrogen, such as metal alloys, metal-organic frameworks and carbon nanotubes etc [8–14]. Because carbon nanotube (CNT) and carbon nanofiber (CNF) have special one-dimensional (1D) nanostructures (resulting in their good dispersibility and operability) and multiaperture geometrical structures (providing a large specific surface) [15], they have been considered as ideal cornerstone materials for improving the capacities of hydrogen storage materials [16–19]. Some works have been conducted to modify the above carbon frameworks, such as titanium, cobalt and magnesium etc [20–22]. Among these materials, metal Co is a desired candidate for absorbing hydrogen [23]. Recently, a series of cobalt–carbon materials [12–14,20,24–26] are reported to have high reversible absorption/desorption hydrogen capacities and good cycle life as negative electrode materials of electrochemical hydrogen storage cells, and their electrochemical hydrogen storage capacities are obviously improved after mixing some nonmetallic materials, as shown in Table 1.

It has been reported that CNT/Co was obtained through a ball-milling treatment at a lower speed of 450 r min^{-1} for 10 h, which reached the capacity of 402.5 mAh g^{-1} (1.48 wt% hydrogen) for electrochemical hydrogen storage [12]. Compared with the theoretical hydrogen storage capacities of individual metal Co (3.32 wt% hydrogen) [31], the capacity obtained is not satisfied, which may be due to efficient grain refinement and the weak composite structures under a lower activation energy provided by a lower speed ball-milling (BM). Considering the reaction between metal Co and carbon materials for Co_3C compound when the ball-milling speed nearing 800 r min^{-1} [12], a suitable ball-milling speed (600 r min^{-1}) is selected in this work to attempt to obtain Co and CNT (CNF) composites with higher hydrogen storage capacity. And it is found that the as-prepared composites (CNT/Co and CNF/Co) exhibit excellent electrochemical hydrogen storage capacity of 717.3 mAh g^{-1} (2.62 wt% hydrogen) and 739.4 mAh g^{-1} (2.70 wt% hydrogen). Also their hydrogen storage processes and the mechanism have been proved as a quasi-reversible CNT (CNF)/Co ↔ CNT (CNF)/Co–H_x reactions happening at three different locations for the dominant cycle process, which was not observed before.

2. Experimental

Metal Co powders (purity 99.9%, 200 mesh, Shanghai Xingzhi chemical factory) were firstly mixed with CNT or CNF (Shenzhen Namigang Co. Ltd.) with the mass ratio of 5:1. In a typical experiment, all samples were ball-milled using a planetary ball mill (pulverisette 7, FRITSCH) in a ZrO_2 vessel at the speed of 600 r min^{-1} for 2–10 h under Ar atmosphere. The mass ratio of ball to powder was maintained at 10:1. After cooling to room temperature, the obtained powders were collected and characterized by X-ray diffraction (Rigaku D/max IIIA, Cu Kα). The scan rate of 0.05° s^{-1} was used to record the patterns in the 2θ range of 10–70°. Scanning electron microscope (SEM) image was obtained by a JSM-6700F field emission scanning electron microanalyser (JEOL, Japan), whereby the powders were mounted on a copper slice. Transmission electron microscopy (TEM) and High-resolution transmission electron microscopy (HRTEM) images were recorded on a JEOL-2010 TEM at an acceleration voltage of 200 kV. The electrochemical measurements were carried out following the method reported with slight modification [43]. Briefly, the electrodes were prepared by mixing CNT/Co or CNF/Co powders, acetylene black and polytetrafluoroethylene at the weight ratio of 7:2:1, which was pressed onto a porous nickel mesh at 50 MPa. Experiments were performed in a two-electrode cell in 6 mol L^{-1} KOH at 25 °C under normal atmosphere, $Ni(OH)_2$ as the counter electrode. The cycle life and charge–discharge curves were tested by a LAND battery-test instrument (CT2001A). The negative electrodes were charged at a current density of 100 mA g^{-1} for 8 h, and then discharged to 0 V at a current density of 30 mA g^{-1}. Furthermore, in order to study the rate capability of the composites, the negative electrodes were discharged to 0 V at current density of 200–1000 mA g^{-1}. The cyclic voltammetry (CV) was conducted by using an electrochemical workstation (CHI660D) of three-electrode test cell. The cell consisted of the composites as the working electrode, metal platinum gauze as the counter electrode, an Ag/AgCl electrode as the reference electrode, and the electrolyte was 6 mol L^{-1} KOH.

Table 1
Preparation methods and hydrogenation capacities of pure Co and cobalt–carbon composites.

Materials	Preparation method	Storage capacity (wt% hydrogen)
Co [24]	Chemical precipitation	1.29
Co–CNT [20]	Ball milling (450 r min^{-1}, 10 h)	1.48
Co_3C [12]	Ball milling	5.176
Graphene–porous cobalt [13]	Chemical precipitation	0.89
Cobalt graphene [14]	Ball milling	3.29
Cobalt–mesoporous carbon [25]	Chemical precipitation	0.45
Cobalt–carbon aerogels [26]	Chemical precipitation	4.38

3. Results and discussion

3.1. Structure and morphology of CNT/Co composite

Firstly, the overall crystalline and purity of the raw materials are investigated by XRD diffraction. As shown in Fig. 1(a), the raw Co powder has two phases: *fcc* phase (PCPDF 15-0806) and *hcp* phase (PCPDF 89-4308). And the XRD pattern of raw CNT displays two strong diffraction peaks at 26.5° and 42.4°, which can be attributed to the hexagonal graphite structures (PCPDF 26-1076). After ball-milling the precursors for several hours at 600 r min^{-1} under Ar atmosphere, it is found that all diffraction peaks corresponding to Co are broadened, as shown in Fig. 1(b) which indicates that the Co crystalline grains are refined. In addition, the transformation of *fcc*-cobalt into *hcp*-phased has also been observed. As reported, that lattice surface energy of *fcc*-Co ($\sim 2.05 \times 10^{-18}$ J per unit lattice) is lower than that of *hcp*-Co ($\sim 2.61 \times 10^{-18}$ J per unit lattice), and *hcp*-Co is a more stable phase [27]. Also the sample's average crystallization size of metal Co is 3.4–4.4 nm calculated by the Scherrer equation from the XRD results, which implies the efficient refinement process in this work.

To investigate the composites' morphologies and composite status and screen out the optimum composite machining condition for their ball-milling preparations, SEM examinations of the ball-milled composites are carried out. Fig. 2(a)–(c) shows the SEM images of pure CNT and CNT/Co composites ball-milled for 4 h and 6 h. It can be seen that uniform 1D composites form and rare individual metal Co particle is observed. It is also found that the diameters of the final products change to ~48 nm after ball-milling the CNT (~40 nm) and metal Co for 4 h and 6 h, respectively, which implies that metal cobalt has been well coated on the surfaces of CNTs. As the ball-milling times are extended from 4 h to 6 h, the CNTs are cut off and their lengths of the 1D product are significantly reduced, as shown in Fig. 2(b) and (c). So the 4 h is the suitable ball-

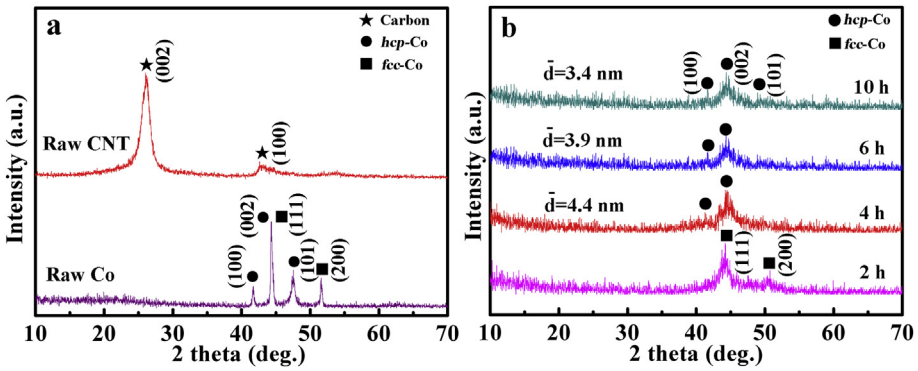

Fig. 1. (a) XRD patterns of the raw metal Co and CNT; (b) XRD patterns of the products of CNT/Co ball-milled by 600 r min^{-1} for 2 h, 4 h, 6 h and 10 h.

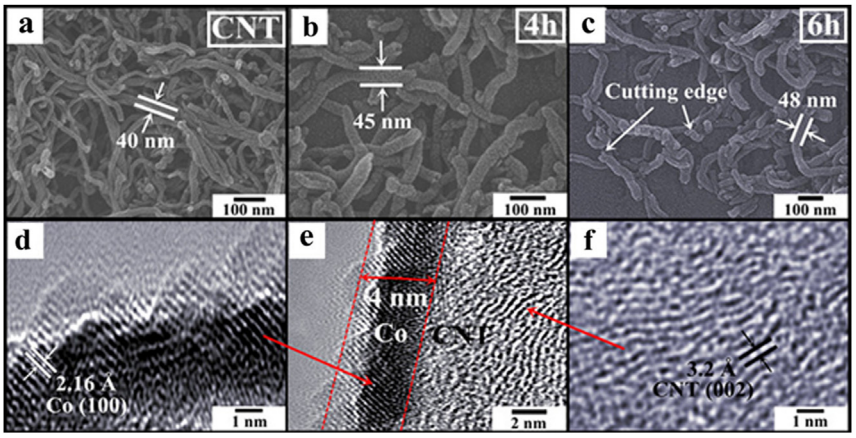

Fig. 2. (a)–(c) SEM images of raw CNT and CNT/Co composites ball-milled for 4 h and 6 h; (d)–(f) HRTEM images of CNT/Co composites after ball-milled for 4 h.

milling time for the preparation in this work. In addition, the composite microstructures of the as-obtained CNT/Co materials ball-milled for 4 h are further investigated through TEM examinations. As shown in Fig. 2(d), a uniform cobalt layer is coated outside the CNT, which implies that the cobalt nanoparticles well expand on the CNT matrixes, forming a shell-like structure. It can be clearly observed that the thickness of cobalt shell is about 4 nm and the shell mainly exposes (100) planes of *hcp*-Co (lattice spacing: 0.216 nm), as shown in Fig. 2(d). There is no crystal plane corresponding to *fcc*-Co found. Due to the smooth surfaces of CNT/Co composite nanotubes and the change of the composites' diameters, the formation process of the Co shell should be a Kossel Stranski two-dimensional nucleation process, which is a layer-by-layer growth [28–30]. It is also found that the particle size of the refined metal Co obtained through a similar ball-milling process, only without the addition of CNT, is more than 100 nm, which proves the high-efficient dispersion and template function of CNT in this work.

3.2. Structure and morphology of CNF/Co composite

As shown in Fig. 3(a), the CNF used in this work is amorphous and there is no obvious diffraction peak observed in its XRD pattern. After ball-milling, it is found in the products' XRD patterns that all diffraction peaks related with metal Co are broadened, indicating a grain refinement process, as shown in Fig. 3(b). In

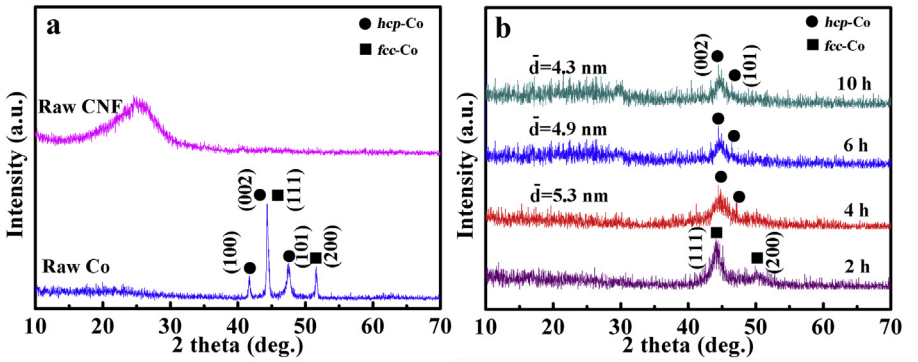

Fig. 3. (a) XRD patterns of the raw metal Co and CNF; (b) XRD patterns of the products ball-milled with 600 r min^{-1} for different hours: 2 h, 4 h, 6 h and 10 h.

addition, it is also found that through the ball-milling treatment all *fcc*-phase Co in the raw material is transformed into *hcp*-phase Co, which is similar to that of CNT/Co. As the previous reports, the ball-to-powder weight ratio, rotate speed and ball milling time synthetically decide the cobalt product's phase. Especially the lower weight ratio and the shorter ball milling time are the proper conditions for *fcc* phase transforming into the *hcp* phase [31–33]. And the samples experience a refinement process, average crystallization size of metal Co is 4.3–5.3 nm, calculated by the Scherrer equation from the XRD results in Fig. 3(b).

In order to explore the expected CNF/Co composite structure, SEM and TEM measurements have been conducted. As shown in Fig. 4(a), the diameter of the raw CNF used in this work is about 8 μm. After ball-milling with Co for 4 h, the 1D product's diameter increases to nearly 10 μm and the surface is smooth. Compared with the thickness of Co shell on the above CNT/Co composite, the thickness of CNF/Co is much larger, which indicates that the size of Co layer is mainly dominated by the size of the templates: CNT or CNF. Furthermore, HRTEM measurement results, as shown in Fig. 4(b)–(d), clearly demonstrate that metal Co has been bestowed on the CNF precursor, forming a core/shell composite structure. The HRTEM images in Fig. 4(d) also reveal that there is only (100) plane of *hcp*-Co exposed, whose lattice spacing is 0.216 nm. As the ball-milling times are extended from 4 h to 6 h, the lengths of the 1D CNF/Co are significantly reduced. Therefore, the 4 h ball-milling should be optimum for Co and CNF composites under this condition, which is similar to the results of CNT/Co.

According to the above results and analysis, the formation processes of CNT/Co and CNF/Co composite structures are illustrated in Scheme 1. Firstly, bulky Co precursor is shattered into small particles and melts through the crashing of the ZrO_2 milling balls, forming Co liquid droplets. After that the droplets freely land on the 1D materials of CNTs' or CNFs' surfaces. Due to the CNTs' and CNFs' good thermal conductivity and mechanical stiffness, liquid Co fast solidify and crystallize, resulting in the formation of the corresponding composites.

3.3. Electrochemical hydrogen storage properties of CNT/Co and CNF/Co composites

In order to investigate their capacities and the stability for electrochemical hydrogen storage, the cycle performances of the composites are examined. Fig. 5(a) shows the capacities and cycle stability of pure CNT electrode and CNT/Co electrodes at a discharge current density of 30 mAh g^{-1}. As shown in Fig. 5(a), the pure CNT and CNT/Co composite ball-milled for 4 h show the maximum storage capacities of about 0.11 wt% hydrogen and 2.62 wt% hydrogen, which is calculated respectively according to the total weight of the composites. Even prolonging the cycle count to 20, the discharge capacity of composite is still 1.41 wt%. However, when the CNT and Co are ball-milled for more than 4 h, the maximum capacity is decreased from the 2.62 wt% hydrogen to 2.49 wt% hydrogen with the decrease of their lengths. This phenomenon agrees with that reported in previous literature: when the cylinder structure of the nanotube was cracked and ruptured, their hydrogen storage capacities would reduce [34]. Therefore, 4 h should be optimum ball-milling time for Co and CNT composites under this condition.

As is known, CNF possesses high electronic conductivity and usefully mechanical properties, which can effectively prevent inner resistance and keep the good cycle performance of the ball-milled composite electrode [35–37]. The hydrogen storage abilities of the above CNF/Co have been further studied in detail. Fig. 5(c) shows the capacities and cycle stability of CNF/Co electrodes under 30 mA g^{-1} discharge current density. Similar to the CNT/Co composites, the pure CNF own a low capacity (0.18 wt%, hydrogen), but the 4 h ball-milling composites show a much higher discharge capacity (2.70 wt% hydrogen), and the discharge capacity can remain 1.41 wt% hydrogen to the highest capacity even after 20 cycles. And it can be seen that the maximum capacity of CNF/Co composite is a little higher than CNT/Co. It has been demonstrated that hydrogen storage capacity of carbon material is proportional to its special surface area and the volume of micropores [44,45]. So the higher capacity of the as-obtained CNF/Co composite should be due

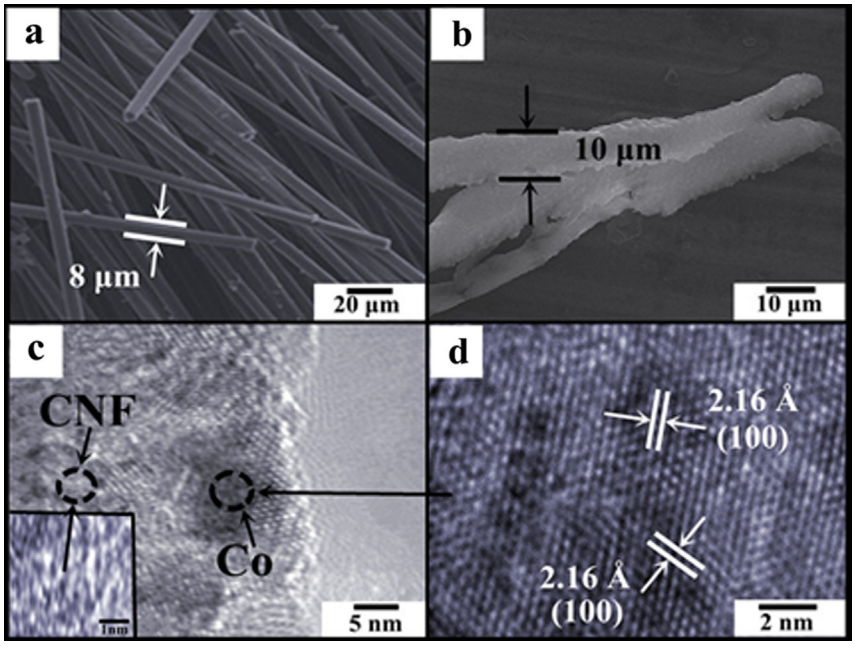

Fig. 4. (a) and (b) SEM images of pure CNF and CNF/Co ball-milled for 4 h; (c) and (d) HRTEM images of CNF/Co ball-milled for 4 h.

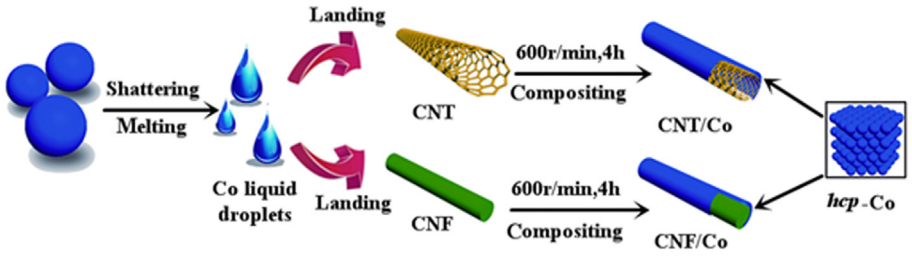

Scheme 1. Illustration of the formation process of core/shell structured CNT/Co and CNF/Co with ball-milling method.

to the existence of many pores in its interior. In addition, Fig. 5(b) and (d) reveal the cycle performance of the CNT/Co and CNF/Co composite electrodes under different current densities: 30, 200, 400, 600, 800 and 1000 mA g^{-1}. It can be seen that the reversible discharge capacity declines with the current density increasing, which has also been found in the previous report [42]. Although the maximum rate capabilities of Co/CNT and Co/CNF both appear at 30 mA g^{-1} current density, the effect of high current density (>200 mA g^{-1}) on them is different. In Fig. 5(b), with the current density increasing, the most satisfying CNT/Co composite ball-milled for 4 h still maintains a high retention rate (>80%). But the retention rate of the CNF/Co composite ball-milled for 4 h exhibits an obvious decrease (<70%) under high current density, as shown in Fig. 5(d). In both CNT/Co and CNF/Co core/shell structured composites, the CNT and CNF play framework roles and the cobalt grains covered on their surfaces reform a seal cylinder, which results in the higher hydrogen storage capacity. Relatively, the hydrogen storage ability of single carbon materials under ambient temperature and pressure is low [8,9], which is mainly due to its rapid escape from the space between carbon skeleton construction [38]. Also the absorption of hydrogen to the exterior of the carbon layer via Van der waals interactions needs a large binding energy to keep steady [10,11].

In order to further investigate the process and mechanism of 1D CNT/Co and CNF/Co core/shell composites for electrochemical hydrogen storage, the relationship between potential and hydrogen storage capacity of CNT (CNF)/Co composite electrode at a discharge current density 30 mAh g^{-1} is investigated, as shown in Fig. 6(a) and (c). Unlike the sandwich-like Co/GE/Co structure composites, both the discharge curve of 1D core/shell composites have three plateaus. The charging voltage plateaus appear at about 1.32 V and 1.43 V (vs. Ag/AgCl electrode), which can be attributed to the reaction of CNT (CNF)/Co → CNT (CNF)/Co–H_x [39]. The composite electrodes have three discharging voltage plateaus, the lowest volt plateau can be attributed to the desorption of hydrogen adsorbed on the surfaces of electrodes [38,40,41]. The special plateau located about 0.7 V can be attributed to the hydrogen stored in hollow structures of the CNT and CNF. Because the capacities are according to the pure CNT and CNF, it also illustrate why the hydrogen store of CNT/Co is little higher than CNF/Co composites. The capacities of this plateau agree with the capacities of pure CNT or CNF, as shown in Fig. 6(a) and (c). The 1.2 V plateau attributes to the bonding state hydrogen and reflects the reaction of CNT (CNF)/Co–H_x → CNT (CNF)/Co. It is also found obviously that this plateau of the composites ball-milled for 4 h is longer than that of the composites ball-milled for 6 h and is the largest contributor to the higher capacities.

Furthermore, cyclic voltammograms (CVs) were also carried out to investigate the electrochemical hydrogen adsorption–deabsorption behaviors of CNT (CNF)/Co composites. Cyclic

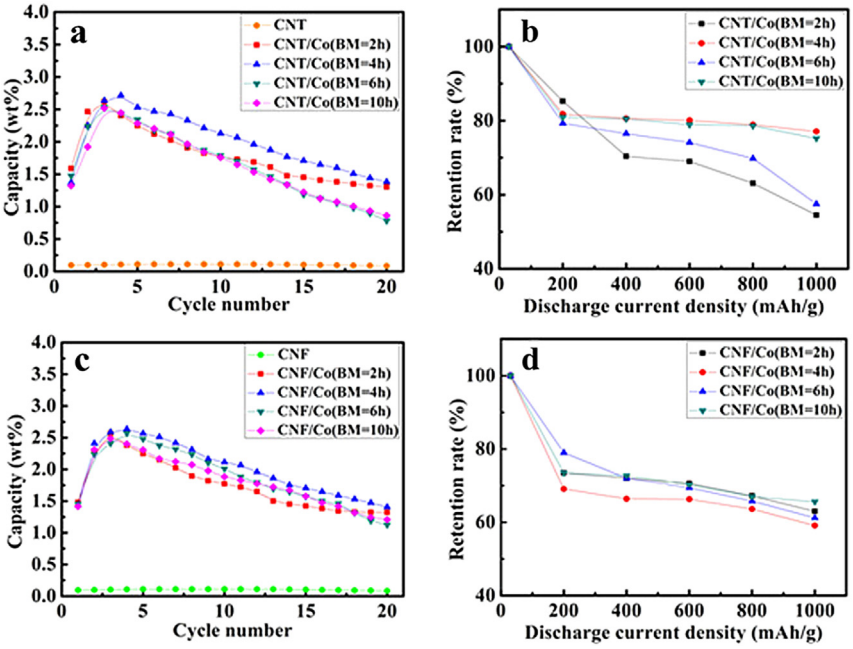

Fig. 5. (a), (c) Cycle performance of CNT (CNF)/Co composites (Co:CNT (CNF) = 5:1, 600 r min^{-1}) for different ball milling hours; (b), (d) Rate capabilities of the CNT/Co composites (Co:CNT (CNF) = 5:1, 600 r min^{-1}) electrodes under various discharge current densities.

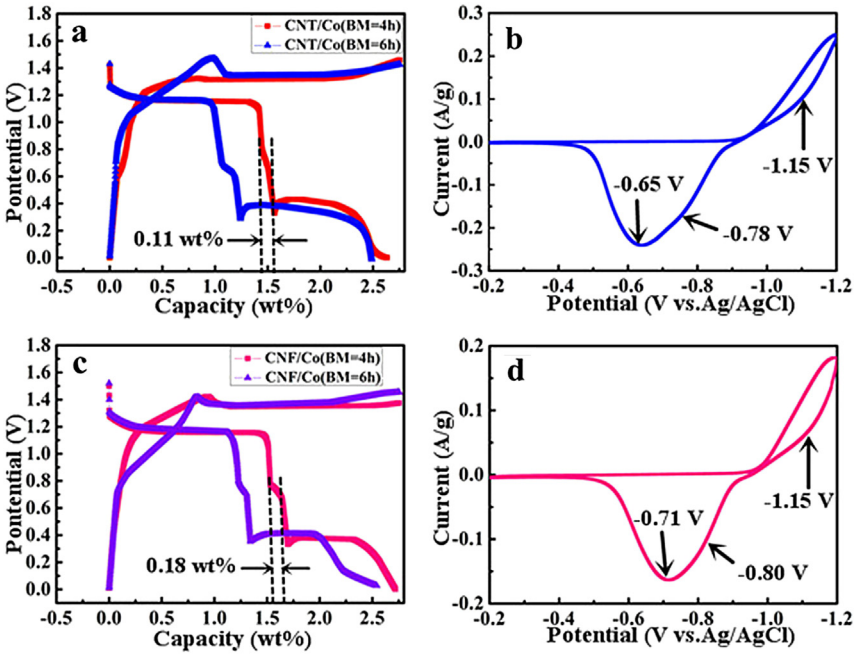

Fig. 6. (a), (c) Charge–discharge curves of the CNT (CNF)/Co composites (BM = 4 and 6 h, 600 r min^{-1}); (b), (d) Cyclic voltammogram curves (scan rate: 5 mV s^{-1}) of the CNT (CNF)/Co composites (BM = 4 h, 600 r min^{-1}).

voltammogram curves of the CNT(CNF)/Co composite ball-milled for 4 h at a scan rate of 5 mV s^{-1} are presented in Fig. 6(b) and (d). Three remarkable peaks are detected. The peak at about −0.70 V can be attributed to the desorption of hydrogen on the products' surfaces, which agrees with the report literature before [42]. There is also another peak near −1.15 V which is attributing to absorption hydrogen process. According to the analysis above, the special peak nears the −0.80 V is belonged to the hydrogen released from CNTs' or CNFs' inner, and the whole electrochemical reaction is as follows:

$$CNT(CNF)/Co + xH_2O + xe^- \leftrightarrow CNT(CNF)/Co - H_x + xOH^-$$

4. Conclusions

As refined nano Co grains are coated on honeycomb geometrical structure of CNT and CNF through ball-milling process, the satisfied 1D core/shell structures are obtained. Accordingly, the hydrogen storage capacities of CNT/Co and CNF/Co are significantly improved and the max reversible capacities of the composites are 717.3 mAh g^{-1} (2.62 wt% hydrogen) and 739.4 mAh g^{-1} (2.70 wt% hydrogen), respectively. It is found that quasi-reversible CNT (CNF)/Co + xH_2O + xe^- ↔ CNT (CNF)/Co–H_x + xOH^- is dominant process and three different hydrogen storage mechanisms are demonstrated, which has never found before. The high electrical conductivity and special core/shell composite structures lead to the excellent electrochemical hydrogen storage property and this research may provide a shortcut for the new cobalt-based or carbon-based hydrogen storage materials.

Acknowledgments

We thank the Program for NCET in University (NECT-10-0049, NECT-13-0754), the Natural Science Foundation of China (Grant No. 21001035, 51272050 and 51072038); the Specialized Research Fund for the Doctoral Program of Higher Education of China (No. 20092304120021); Harbin Sci-Tech. Innovation Foundation (RC2012XK017012); Harbin Key Sci-Tech Project (No. 2010AA4BG004); the Fundamental Research funds for the Central Universities (No. HEUCF201210006 and 2014); Outstanding Youth Foundation of Heilongjiang Province (Grant No. JC201008) for the financial support of this research.

References

[1] D. Ravnsbæk, L.H. Sørensen, Y. Filinchuk, F. Besenbacher, T.R. Jensen, Angew. Chem. Int. Ed. 51 (2012) 3582–3586.
[2] L. Schlapbach, A. Züttel, Nature 41 (2001) 353–358.
[3] B. Bogdanovic, M. Felderhoff, S. Kaskel, A. Pommerin, K. Schlichte, F. Schüth, Adv. Mater. 15 (2003) 1012–1015.
[4] P. Chen, Z.T. Xiong, J.Z. Luo, J.Y. Li, K.L. Tan, Nature 420 (2002) 302–304.
[5] W. Lubitz, B. Tumas, Chem. Rev. 107 (2007) 3900–3903.
[6] T.B. Marder, Angew. Chem. Int. Ed. 46 (2007) 8116–8188.
[7] T.K.A. Hoang, D.M. Antonelli, Adv. Mater. 21 (2009) 1787–1800.
[8] A.C. Dillon, M.J. Heben, Appl. Phys. A: Mater. Sci. Process. 72 (2001) 133–142.
[9] A. Züttela, P. Sudana, Ph. Maurona, T. Kiyobayashib, Ch. Emmeneggera, Int. J. Hydrogen Energy 72 (2002) 203–212.
[10] T. Yidirim, S. Ciraci, Phys. Rev. Lett. 94 (2005) 175501.
[11] S.A. Shevlin, Z.X. Guo, Appl. Phys. Lett. 89 (2006) 153104.
[12] P. Gao, Y. Wang, S.Q. Yang, Y.J. Chen, Z. Xue, L.Q. Wang, G.B. Li, Y.Z. Sun, Int. J. Hydrogen Energy 37 (2012) 17126–17130.
[13] Y.J. Chen, Q.S. Wang, C.L. Zhu, P. Gao, Q.Y. Ouyang, T.S. Wang, Y. Ma, C.W. Sun, J. Mater. Chem. 22 (2012) 5924–5927.
[14] S.Q. Yang, P. Gao, D. Bao, Y.J. Chen, L.Q. Wang, P.P. Yang, G.B. Li, Y.Z. Sun, J. Mater. Chem. A 1 (2013) 6731–6735.
[15] P. Serp, M. Corrias, P. Kalck, Appl. Catal. A 253 (2003) 337–340.
[16] W.J. Rieter, K.M. Taylor, W. Lin, J. Am. Chem. Soc. 219 (2007) 9852–9855.
[17] V. Vamvakaki, K. Tsagaraki, N. Chaniotakis, Anal. Chem. 78 (2006) 5538–5542.
[18] C. Kim, B.T.N. Ngoc, K.S. Yang, M. Kojima, Y.A. Kim, Y.J. Kim, M. Endo, S.C. Yang, Adv. Mater. 19 (2007) 2341–2346.
[19] C. Kim, Y.I. Jeong, B.T.N. Ngoc, K.S. Yang, M. Kojima, Y.A. Kim, M. Endo, J. Lee, Small 3 (2007) 91–95.
[20] H.M. Du, L.F. Jiao, Q.H. Wang, W.X. Peng, D.W. Song, Y.J. Wang, H.T. Yuan, J. Power Sources 196 (2011) 5751–5755.
[21] T. Yildirim, Adv. Mater. Process. 163 (2005) 30.
[22] B.H. Chen, C.H. Kuo, J.R. Ku, P.S. Yan, C.J. Huang, M.S. Jeng, J. Alloy. Compd. 15 (2013) 78–83.
[23] B.S. Haran, B.N. Popov, R.E. White, J. Electrochem. Soc. 145 (1998) 3000–3007.
[24] S.R. Chung, K.W. Wang, M.H. Teng, T.P. Perng, Int. J. Hydrogen Energy 34 (2009) 1383–1388.

[25] C.C. Huang, Y.H. Li, Y.W. Wang, C.H. Chen, Int. J. Hydrogen Energy 38 (2013) 3994–4002.
[26] H.Y. Tian, C.E. Buckley, D.A. Sheppard, M. Paskevicius, N. Hanna, Int. J. Hydrogen Energy 35 (2010) 13242–13246.
[27] F.D. Lamari, D. Levesque, Carbon 49 (2011) 5196–5200.
[28] M. Substyk, Cryst. Res. Technol. 23 (1988) 1443–1447.
[29] R. Winand, Hydrometallurgy 29 (1992) 567–598.
[30] R. Winand, Electrochim. Acta 39 (1994) 1091–1105.
[31] J. Sort, A. Zhilyaev, M. Zielinska, J. Nogués, S. Surinach, J. Thibault, M.D. Baro, Mater. Acta 51 (2003) 6385–6393.
[32] J.Y. Huang, Y.K. Wu, H.Q. Ye, K. Lu, Nanostruct. Mater. 6 (1995) 723–726.
[33] P. Tolédano, G. Krexner, M. Prem, H.P. Weber, V.P. Dmitriev, Phys. Rev. B 64 (2001) 144104.
[34] F. Liu, X.B. Zhang, J.P. Cheng, J.P. Tu, F.Z. Kong, W.Z. Huang, C.P. Chen, Carbon 41 (2003) 2527–2532.
[35] J.H. Lee, K.Y. Rhee, S.J. Park, Int. J. Hydrogen Energy 35 (2010) 7850–7857.
[36] C. Park, C.D. Tan, R. Hidalgo, R.T.K. Baker, N.M. Rodríguez, J. Phys. Chem. B 102 (1998) 4253–4255.
[37] J.S. Huang, Y. Liu, T.Y. You, Anal. Methods 2 (2010) 202–211.
[38] Y. Yürüma, A. Taralpa, T.N. Veziroglub, Int. J. Hydrogen Energy 34 (2009) 3784.
[39] Y.H. Zhang, L.F. Jiao, H.T. Yuan, Y.Y. Zhang, L. Liu, Y.J. Wang, Int. J. Hydrogen Energy 33 (2008) 1317–1322.
[40] G.P. Dai, C. Liu, M. Liu, M.Z. Wang, H.M. Cheng, Nano Lett. 2 (2002) 503–506.
[41] X.Y. Zhao, L.Q. Ma, X.D. Shen, J. Mater. Chem. 22 (2012) 277–285.
[42] Y.L. Cao, W.C. Zhou, X.Y. Li, X.P. Ai, X.P. Gao, H.X. Yang, Electrochim. Acta 51 (2006) 4285–4290.
[43] H. Lee, J. Ihm, M.L. Cohen, Nano Lett. 10 (2010) 793–797.
[44] H.M. Cheng, C. Liu, Y.Y. Fan, F. Li, G. Su, H.T. Cong, L.L. He, M. Liu, Z. Metallkd. 91 (2000) 306–310.
[45] W.C. Xua, K. Takahashia, Y. Matsuoa, Y. Hattoria, M. Kumagaia, S. Ishiyamab, K. Kanekoc, S. Iijimad, Int. J. Hydrogen Energy 32 (2007) 2504–2512.